

Time-domain flaw imaging system

L. Medina

*Departamento de Ingeniería de Sistemas Computacionales y Automatización,
Instituto de Investigaciones en Matemáticas Aplicadas y Sistemas, UNAM,
Circuito Escolar, Ciudad Universitaria, 04510, México D.F., México,
e-mail: lucia@uxdea4.iimas.unam.mx*

Recibido el 7 de julio de 2004; aceptado el 23 de noviembre de 2004

Ultrasonic Non Destructive Evaluation of materials is a useful tool for flaw detection and characterization. A typical ultrasonic imaging system may consist of a single transducer or an array of sensors working in a B-scan mode. This mode operates by transmitting a pulse of train of pulses from several locations and detecting the echoes coming from in-homogeneities. The reflected energy can be represented as a map of ultrasonic reflectivity. A time-delay beamformer has been successfully used to reconstruct the image, and localize the in-homogeneities within the scanned medium, by time shifting the signals, and summing them up. This process enables to locate regions at which signals are added constructively. It is however, a time consuming process and requires $\lambda/2$ distance of motor steps or inter-element distance between array elements. An algorithm based on time-domain envelope beamformer is presented here. This algorithm is able to diminish the number of computational operations without losing relevant information about the location of in-homogeneities. A comparison between classical and envelope beam-formers is presented when applied to sets of simulated signals. Lateral and longitudinal resolutions are also computed when two targets are within the scanned medium.

Keywords: Synthetic aperture focusing technique; time-domain beam-forming technique; flaws location.

Ensayos no destructivos con ultrasonido es una herramienta comúnmente usada para la detección y caracterización de fallas en materiales. Un sistema típico de imágenes ultrasónicas consiste en un solo transductor o arreglo de sensores que operan bajo el modo de rastreo B. Este modo consiste en transmitir un pulso o un tren de pulsos desde distintas posiciones, y para cada posición recibir ecos que pueden provenir de inhomogeneidades dentro del material inspeccionado. La energía reflejada puede desplegarse como un mapa de intensidades ultrasónicas. Uno de los métodos que han tenido gran éxito en la reconstrucción de imágenes y localización de inhomogeneidades es la llamada formación de haces, proceso digital en el dominio del tiempo. Esta técnica consiste en aplicar corrimientos en el tiempo específicos a cada señal registrada, para después sumar éstas, encontrando así las zonas donde las señales se suman constructivamente. Sin embargo, esta técnica requiere largos periodos para su procesamiento así como la restricción de la distancia entre elementos no debe exceder de $\lambda/2$. El trabajo que se presenta propone un algoritmo en el dominio del tiempo, que opera sobre la envolvente de las señales recibidas, disminuyendo el número de operaciones computacionales sin perder información relevante de la localización de inhomogeneidades. Resultados comparativos entre la técnica clásica y la propuesta son presentados cuando ambas son aplicadas a un conjunto de señales simuladas. También resoluciones laterales y longitudinales han sido calculadas en el caso de que existan dos fallas puntuales en el medio inspeccionado.

Descriptores: Técnica de focalización de apertura sintética; técnica de formación de haces en el dominio del tiempo; localización de fallas.

PACS: 43.60.+d; 43.60.Gk; 43.35.Sx

1. Introduction

Ultrasonic B-scan imaging has been successfully used in medical diagnosis, nondestructive testing, and underwater imaging. Currently, the most popular method to obtain an image is the pulse-echo method. A pulse-echo ultrasonic imaging system consists either of a single transducer, or a set of sensors conforming an array. These sensors transmit a pulse or train of pulses through the propagation medium. If the transmitted ultrasonic wave encounters a specimen, with different acoustic impedance respective to the propagation medium, energy is reflected; then an echo is produced and detected by the transducer or transducers.

The longitudinal and lateral resolutions of the method depend on the duration of the ultrasonic signal and the size of the transducer. If a large transducer is used, the lateral ambiguity increases. If the ultrasonic beam is wider it would result in a poor performance in the far-field region. To overcome these limitations, the synthetic aperture focusing technique (SAFT) has been developed [1–4]. This technique co-

herently combines pulse-echo measurements made at several transmitter/receiver locations to form a map of ultrasonic reflectivity of the radiated region. SAFT takes the advantage of both spatial and temporal resolution correlations to enhance the resolution and signal-to-noise ratio of the reconstructed images.

The multiple transmitter/receiver locations have been performed either by using a single transducer mechanically moved to scan one or two-dimensional apertures [5, 6], or by using an array of sensors [7, 8] or a mechanically moved array [9].

In this study, the time domain has been adopted to reconstruct the ultrasonic image. A comparison between classical and envelope beamformers has been performed. The simulation approach presented in this work is based on:

- the echoes are detected by an array of sensors equally-spaced,
- the targets are considered to be point sources, and
- each array element has a visible region of 120° .

A comparison of lateral and longitudinal resolutions, when two point sources are in the propagation medium between classical and envelope beamformer is also presented.

The theoretical considerations about classical and envelope beamformers, including range and bearing resolutions, are explained in Sec. 2. Section 3 is focused on the simulation of received signals. The results of the beamformers outputs, for a single and two targets present in the propagation medium, are outlined in Sec. 4.

2. Theory

A propagating signal contains relevant information about the source that produced it. The temporal and spatial characteristics combined with the laws of physics frequently enable us to determine the location of the signal source.

One of the most common and simplest range finding technique relies on measurement of time-of-flight (TOF), which is the time taken for the wave to travel from the transmitter to the receiver after being reflected by a target. Range finder techniques used in radar, sonar, and ultrasonic rely on this principle. If the speed of energy propagation (c) in the propagation medium is known, then the distance specimen- n th sensor (r_n) can be measured from:

$$r_n = \frac{1}{2}c\tau_n, \tag{1}$$

where τ_n is the time of flight respective to the n th receiver position or array element. If a single fixed transducer is used, the only information about the target bearing is whether or not the object lies within the visible region of the transducer. An additional process must be carried out to determine the angular position of the target or specimen, such as the beam-forming technique. The beam-former defined as a filtering process [10] could be applied in the time domain [11] or in the frequency domain [12, 13], depending on the hardware trade offs and spectral areas of application.

2.1. Beam-forming Technique

The beam-steering process consists of a phase shifting the signals transmitted or received by an array of elements in incremental angular steps. This is done to find the angles at which the wave incident to an array comes from. The relative phases between elements are adjusted by controlling the progressive phase differences between them, which depend on the difference on the propagation paths. These will scan the array towards the direction of maximum radiation [14]. This process is the same when the array is transmitting or receiving, which was shown experimentally by Munro [15].

Delay-and-sum beam-forming technique [11] uses the appropriate delay, and applies it to the received signals to achieve focusing, and it allows the direction of arrival of the energy onto the transducer or the array of sensors being determined. This method consists of applying time delays to the received signals and then adding them together in order

to find the points at which the received signals are in phase. The schematic process is shown in Fig. 1, and can be expressed as

$$B(t) = \sum_{n=1}^N w_n y_n(t - \Delta t_{F_n}), \tag{2}$$

where y_n is the n th output signal, N is the total number of elements, w_n is the amplitude weight, and Δt_{F_n} is the time delay applied to y_n . The range of summation is determined by the width of the ultrasonic pulse [16], w_n 's are applied to achieve a desired spatial response of the receivers; if no allowance was made for mutual coupling between them, then w_n becomes a unity. Δt_{F_n} required to steer the beam to the specified direction, is directly related to the length of time takes for the signal to propagate between sensors [11], and is given by

$$\Delta t_{F_n} = 2 \frac{|r_{F_n}|}{c} = 2 \frac{|r_F - \mathbf{x}_n|}{c}, \tag{3}$$

where $|r_{F_n}|$, and $|r_F|$ are the focal distances from n th receiving position (x_n), and reference point to the focusing point, respectively. Figure 2 shows the geometric information needed to calculate n th Δt_F .

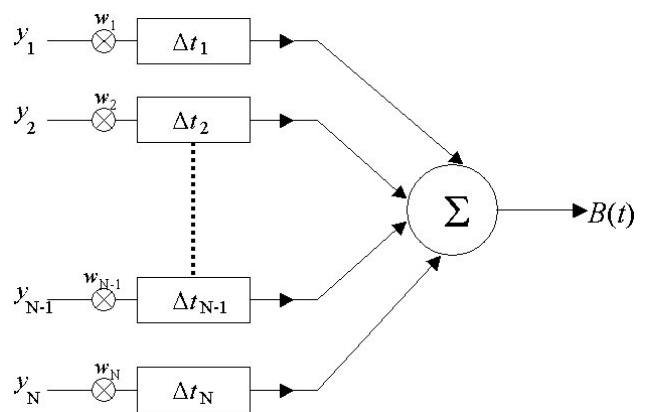


FIGURE 1. Time-delay beamforming process.

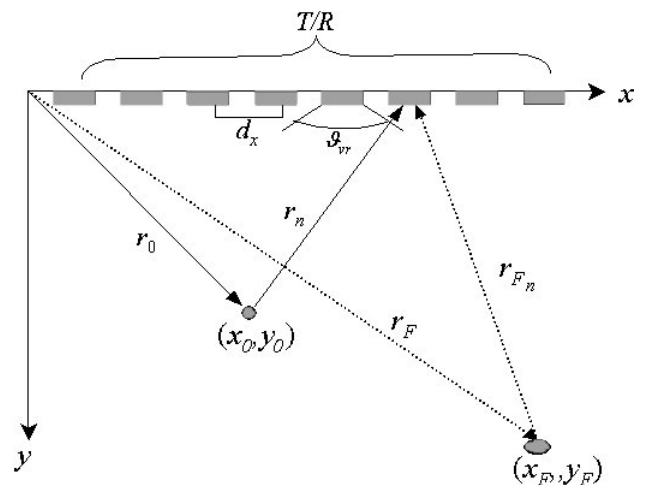


FIGURE 2. 2D region of interest.

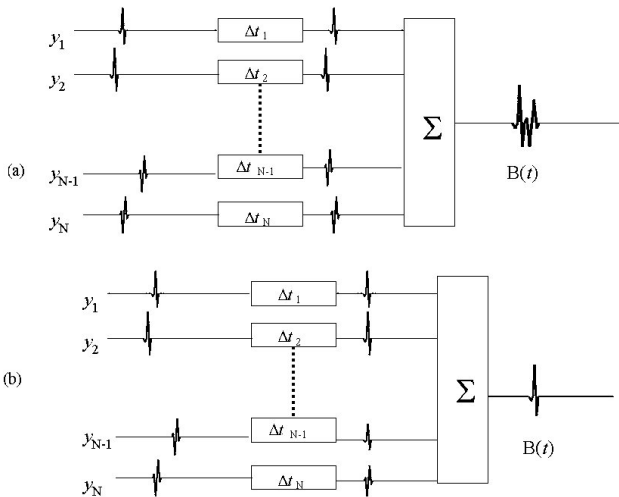


FIGURE 3. Digital beam steering and focusing: a) at the wrong direction and b) at the direction of maximal energy.

If the beam-former focuses the array in the wrong direction, the result is a degraded version of the propagation signal, as it is shown in Fig. 3a. In this case the beam-former is mismatched to the propagation wave [17]. There are two possible reasons for this mismatch, one is that the assumed direction of propagation does not equal the true direction of propagation, and the second is that the speed of sound in the medium is wrongly determined.

If the beam-former focuses the array in the desired direction (Fig. 3b), the propagation delays are added constructively, giving the correct direction of maximum radiation, and therefore the position of the target is found.

When the beam is not steered, grating lobes may appear if the elements are spaced more than $\lambda/2$ (λ is the wavelength), in analogy to slits in optics [18]. This requirement can be eliminated when short pulses are used, and the beamforming process is applied to the envelope of received signal [19,20].

2.2. Envelope Beamforming Technique

A new approach to the classical beamforming technique was developed by Webb [19], for a pick-and-place robot operation. This modified algorithm filters, delay and sums the output signals of finite length. The signals which consist of a few cycles of the wave are envelope detected and can be approximated by

$$y(t) = \begin{cases} a(t) \cos \omega t & -\frac{t_p}{2} \leq t \leq \frac{t_p}{2} \\ 0 & \text{otherwise,} \end{cases} \quad (4)$$

where $a(t)$ is the envelope of the signal, where amplitude modulate the function $\cos \omega t$, and t_p is the pulse length. The total energy, a non-periodic function, received by the array is

$$E = \sum_{n=1}^N E_n = \sum_{n=1}^N y_n(t + \tau_{F_n}), \quad (5)$$

where E_n is the energy received at the n th array element and

$$\tau_{F_n} = 2 \frac{\sqrt{(x_F - x_n)^2 + y_F^2}}{c}, \quad (6)$$

and x_F and y_F are the focal point coordinates, and x_n is the transducer position, as shown in Fig. 2.

The advantages of this technique compared to the classical beam-forming method are that the signals are added constructively only in one summation, and restriction of $\lambda/2$ inter-element distance disappear. Also the number of computational operations is diminished.

2.3. Range Resolution

A system range resolution may be defined as:

- a) Two targets are resolvable when the distance between them is at least half of the pulse length r_p [15], as shown in Fig. 4. The pulse length in time ($t_p = r_p/c$), is given by the Bandwidth Theorem [21] as

$$\Delta f_{3dB} \cdot t_p \approx 1, \quad (7)$$

where Δf_{3dB} is the pulse bandwidth at 3 dB's. Then the range resolution, as the minimum distance between two targets, because it is a band-limited signal [22], is given by

$$r_{r|p} = \frac{c}{2\Delta f_{3dB}} = \frac{ct_p}{2} = \frac{r_p}{2}. \quad (8)$$

The smaller the pulse, the better the range resolution of the system, and

- b) The range resolution defined as the smallest change detected in range, depends on the sampling rate (f_s) at which the signal is acquired. By the Shannon's Sampling Theorem [23], f_s has to be at least twice the frequency at which the pulse is produced. The minimum acquired distance given by the sampling rate is

$$r_r = ct_s = \frac{f}{f_s} \lambda, \quad (9)$$

where t_s is the time elapsed in a single sample.

2.4. Bearing Resolution

The bearing resolution of an array [15], based on the Rayleigh criterion [18], states that "two components of equal intensity should be considered resolved just when the principal intensity maximum of one coincides with the intensity minimum of the second one". The angle subtended by the sources at the receiver, θ_r , is called the angle of resolution. Hence, if two wavefronts are incident on the array, one along the normal ($\theta = 0$) of the array, and the other at angle θ_r to the normal, then their central maxima and first minima generated from the beam steering process would coincide. The angular resolution, based on Rayleigh criterion, is given as

$$\theta_r = \sin^{-1} \left(\frac{\lambda}{Nd_x} \right) = \sin^{-1} \left(\frac{\lambda}{b_x} \right), \quad (10)$$

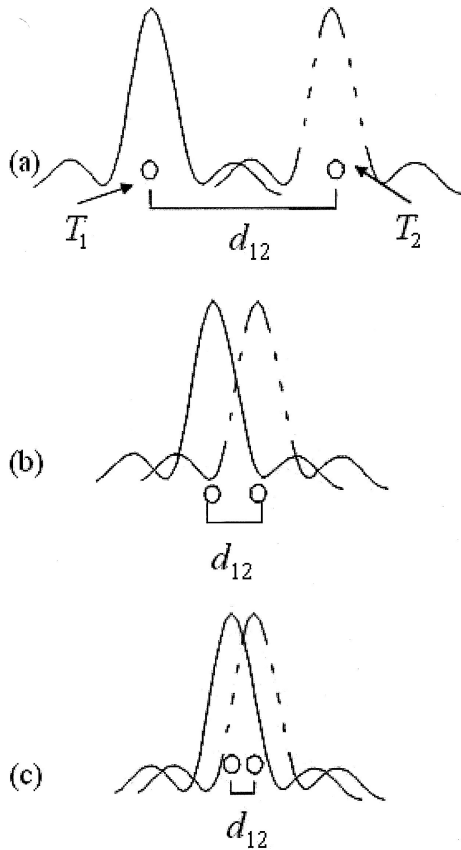


FIGURE 4. Range resolution: a) $d_{21} > r_p/2$, b) $d_{21} = r_p/2$ and c) $d_{21} < r_p/2$.

where d_x , and b_x are the inter-element distance and array aperture. Thus, the larger the array aperture, the better the angular resolution. Also, to compute the bearing resolution, it is necessary to consider other factors such as: the sampling rate, and the time delay inserted in the output signals in the beam-forming process. The minimum time delay that can be inserted is t_s , which corresponds to one sample. Then the angular resolution is

$$\theta_r = \sin^{-1} \left(\frac{ct_s}{|\mathbf{x}_n|} \right) = \sin^{-1} \left(\frac{r_r}{|\mathbf{x}_n|} \right). \quad (11)$$

The larger the distance between the n th-element to the point of reference, the better the angular resolution.

The bearing resolution used in this work is considering that the minimum distance at which two targets can be resolved is given by Eq. (8). Based on this, the minimum angle at two targets can be distinguished by the system (see Fig. 5) and calculated as

$$\theta_r = \cos^{-1} \left(\frac{d_{1n}^2 + d_{2n}^2 + r_{r|p}^2}{2d_{1n}d_{2n}} \right), \quad (12)$$

where d_{1n} , and d_{2n} are the distances between targets and the point of reference.

3. Simulation

The echo received by the transducer at the n th position can be represented as a delay version of the transmitted pulse $y(t)$, as

$$y_n(t) = \frac{y(t - \tau_n)}{|\mathbf{r}_n|} = \frac{y(t - 2|\mathbf{r}_0 - \mathbf{x}_n|/c)}{|\mathbf{r}_0 - \mathbf{x}_n|}. \quad (13)$$

If the transmitted pulse is considered as a harmonic summation represented as the convolution between an envelope and the spherical wave, then $y(t)$ can be written as

$$y(t) = \frac{a(t)}{|\mathbf{r}_0|} \exp^{i\omega t}. \quad (14)$$

The received signal is detected after the transmitted pulse has travelled from the transmitter to the receiver after being reflected by the target, and is acquired at a sampling rate given by the Shannon's theorem. Other important parameter is the visible region (θ_{vr}), which depends on the size and shape of the transducer. When a pulse is transmitted through the medium of propagation, the region of illumination can be represented as a cone of certain angle. This angle is then used to define the visible region of the transducer, as shown in Fig. 2.

If the pulse length is 5 cycles, $a(t)$ is considered as a Gaussian window, the carrier frequency is $f = 1.5MHz$, and the signal is acquired at a sampling rate of $f_s = 3f$, then the received signals can be simulated as the real part of Eq. (13), as shown in Fig. 6.

3.1. Additive White Noise

The signal, transmitted and received, is contaminated along the path by undesirable signals [24], called noise, which are random and unpredictable signals produced externally or internally. By careful engineering, the effects of many unwanted signals can be reduced, but there always remain certain random signals. Noise that contains all frequency com-

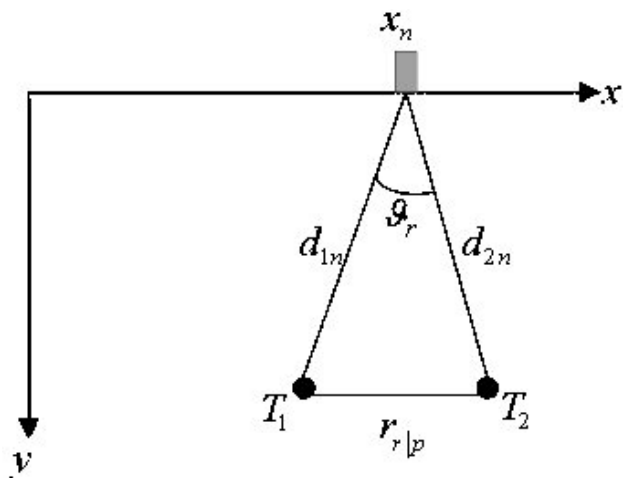


FIGURE 5. Bearing Resolution.

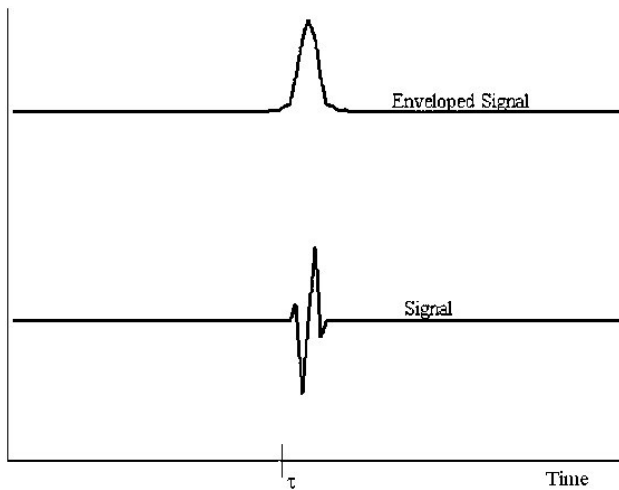


FIGURE 6. Simulated signal (lower), and its envelope (upper).

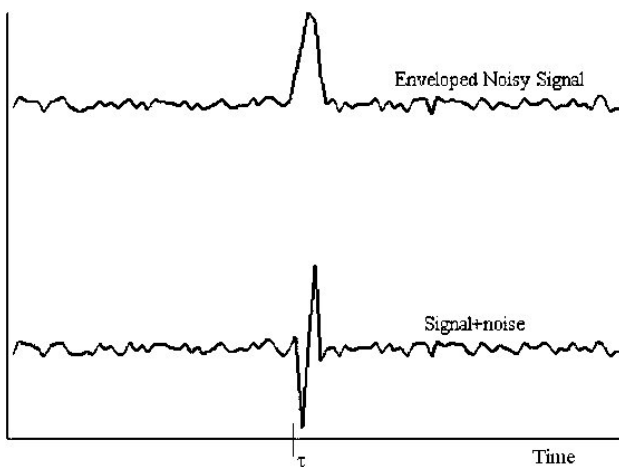


FIGURE 7. Simulated received signal with additive white noise (lower) and its envelope (upper).

ponents in equal proportion is called white noise. The white noise is considered to be a Gaussian process of mean zero [25]. If white noise is added to the received signal, it becomes a random signal, given by

$$s_n(t) = y_n(t) + n(t). \quad (15)$$

A simulated noisy signal and its envelope are plotted in Fig. 7.

4. Results

Classical and envelope beamformer algorithms have been developed and applied to simulated signals. The analysis has been made varying the pulse length, and also considering noiseless and noisy signals. In order to measure the range resolution of the system for each length, the results are split into two:

- a) single target detection, and

TABLE I. Digital signal simulation parameters.

Parameter	Value
f	1.25 MHz
c	1500 m/s
λ	1.2 mm
f_s	3.75 MHz
N	100
d_x	$\lambda/2$
$a(t)$	Gaussian
θ_{vr}	120°
$r_p(t_p = r_p/c)$	1.5 λ , 3 λ and 5 λ

TABLE II. Digital beamformer parameters.

Parameter	Value
r_r	0.4 mm
Lateral Step Distance Δx_F	$\lambda/8$
Longitudinal Step Distance Δy_F	r_r
Lateral Maximum Distance	60.6 mm
Longitudinal Maximum Distance	40.0 mm

- b) range and bearing resolutions when second target is detected. Even though that the algorithms are able to detect $N - 1$ targets.

The results presented here are based on the simulation of received signals detected by an array of sensors. The simulation and digital parameters are defined in Table I and Table II, respectively.

4.1. Single Target Location

A single point target located at [24mm, 10mm] in a 2D space of 60.6 \times 40.0 mm², and N point transducers located along the x -axis, are the data used to calculate the time of flight, given by Eq. (1) for each element. The non-attenuated signals and their envelopes, for each pulse length, are in Fig. 8. These images show the time-of-flight foci, represented as a hyperbolic-shaped curve.

To locate the position of the target, the classical and the envelope beamforming algorithms were applied to the simulated signals, and the target is clearly located as shown in Fig. 9. Figs. 9a, 9b, and 9c are the time delay beamformer output, for different pulse lengths, and Figs. 9d, 9e and 9f show the output when the digital process is applied to the envelope of the signals for the same pulse lengths. The main difference between the outputs of both beamformers is the presence of spurious lobes about the maximal energy in the classical technique. The target location must coincide with the position of maximal amplitude of the beamformers output. Table III summarizes the error between the theoretical and the calculated target position.

TABLE III. Lateral (σ_x) and longitudinal (σ_y) errors in a single target location: i) classical and ii) envelope beamformers outputs.

$r_p[\lambda]$	Noiseless Signals				Noisy Signals			
	σ_x [mm]		σ_y [mm]		σ_x [mm]		σ_y [mm]	
	(i)	(ii)	(i)	(ii)	(i)	(ii)	(i)	(ii)
1.5	0.1	0.0	0.2	0.6	0.1	0.0	0.2	0.6
3.0	0.3	0.0	0.4	0.4	0.3	0.0	0.4	0.4
5.0	0.1	0.0	1.6	1.1	0.1	0.1	1.6	1.2

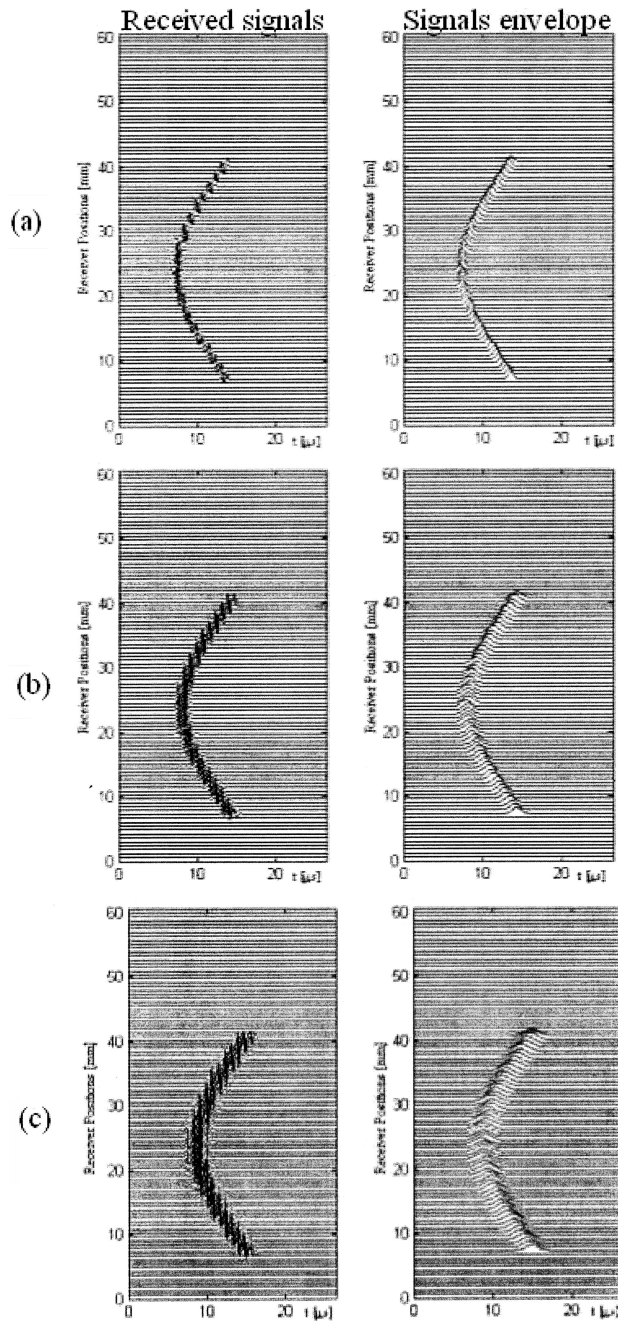


FIGURE 8. Simulated signals when: i) $r_p = 1.5\lambda$, ii) $r_p = 3\lambda$, and iii) $r_p = 5\lambda$.

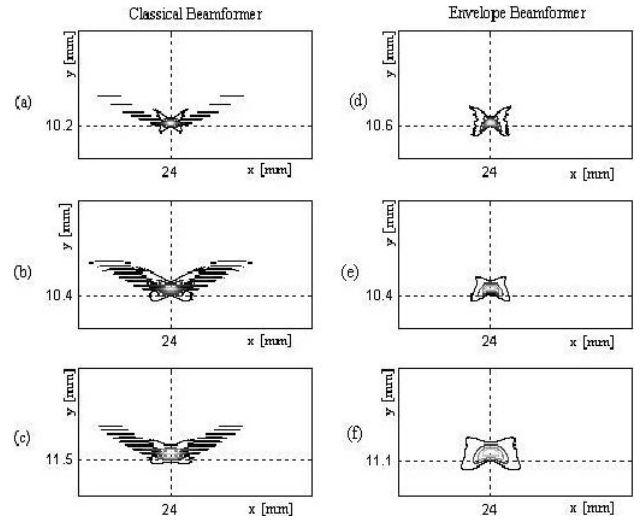


FIGURE 9. Single target detection. Classical Beamformer: a) $r_p=1.5\lambda$, b) $r_p = 3.0\lambda$, and c) $r_p = 5.0\lambda$. Envelope Beamformer: d) $r_p = 1.5\lambda$, e) $r_p = 3.0\lambda$, and f) $r_p = 5.0\lambda$.

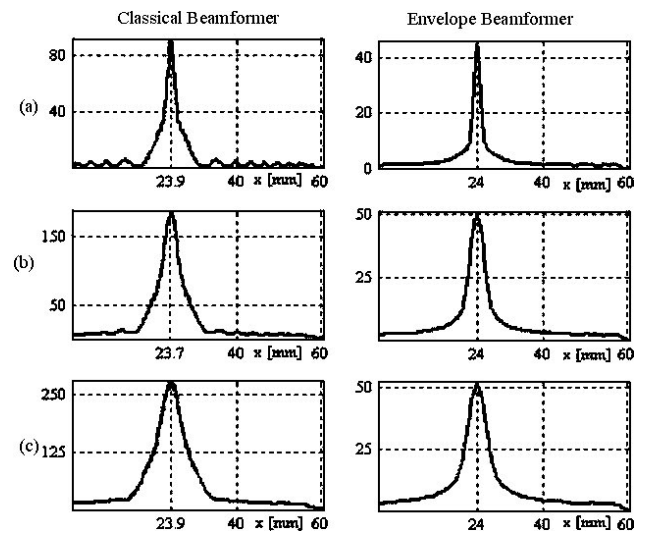


FIGURE 10. Lateral profiles at maximum amplitude: a) $r_p = 1.5\lambda$, b) $r_p = 3\lambda$, and c) $r_p = 5\lambda$.

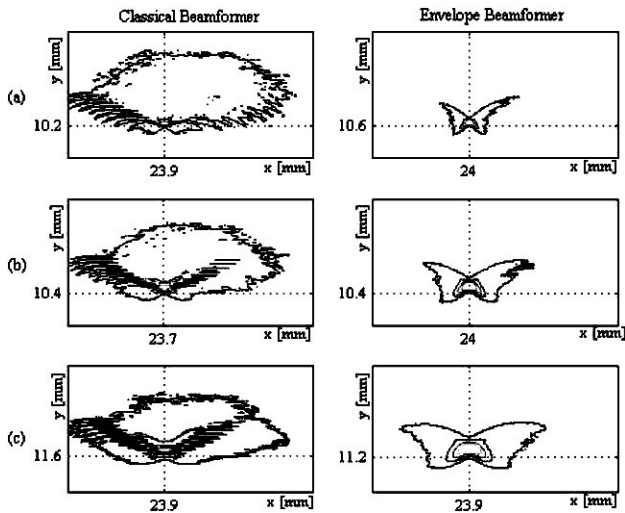


FIGURE 11. Single target detection when signals are contaminated with white noise: a) $r_p = 1.5\lambda$, b) $r_p = 3\lambda$, and c) $r_p = 5\lambda$.

The errors between the theoretical and calculated target positions σ_x and σ_y are within the range resolution of the system, r_r , with the exception of the signals simulated when $r_p = 5\lambda$. The lateral profiles of the beamformers at the maximal energy point are plotted in Fig. 10. The first column of Fig. 10 shows the profiles of a classical beamformer output, the profiles are not as smooth and sharp as the envelope beamformer case, and their shapes are wider than the ones produced by the proposed algorithm. If white noise is added to the received signal, the target location is not substantially affected as summarized in Table III, however the spurious lobes, in the classical technique, about the maximal amplitude region drastically increase (see Fig. 11).

4.2. Two Targets: Range Resolution

In order to measure the range resolution of the system, defined in Sec. 2.4, the simulation was developed considering two different cases:

- a) Lateral range resolution.- A target T_1 was fixed at [29.4mm, 10.0mm], a second target T_2 , was located at several point coordinates within the 2D space, where the x -axis of T_2 was moved from 29.4mm to 12.0mm at $\lambda/2$ steps, and the y -axis had been fixed at 10mm.
- b) Longitudinal Resolution.- A target T_1 was fixed at [29.4mm, 10.0mm], a second target T_2 , was located at several point coordinates within the 2D space, where the y -axis of T_2 was moved from 10.0mm to 16.2mm at $\lambda/2$ steps and the x -axis had been fixed at 29.4mm.

The lateral and longitudinal resolutions were determined by processing the classical and envelope algorithms with the simulated received signals, iteratively. For every iteration, the region of maximal amplitude of the beamformer outputs was calculated. The existence of a two well-defined peaks corresponding to the target positions were determined. If the

beamformer output does not contain information about the second target, then T_2 has to be further away form T_1 , and the digital process has to be applied to the signals.

Lateral resolutions for both algorithms and pulse lengths, considering noiseless and noisy signals, are shown from Fig. 12 to Fig. 14, and the theoretical and calculated resolutions are in Table IV. The theoretical resolution is given by Eq. (8), and the calculated resolution is computed by the distance between the two targets.

TABLE IV. Two targets lateral resolutions: a) Theoretical values, b) Classical and c) Envelope beamformers.

$r_p/2$ [mm]	r_x [mm]			
	Noiseless Signals		Noisy Signals	
(a)	(b)	(c)	(b)	(c)
0.9	1.8	3.0	3.6	3.0
1.8	3.6	4.9	3.7	4.8
3.0	5.5	6.4	5.8	6.4

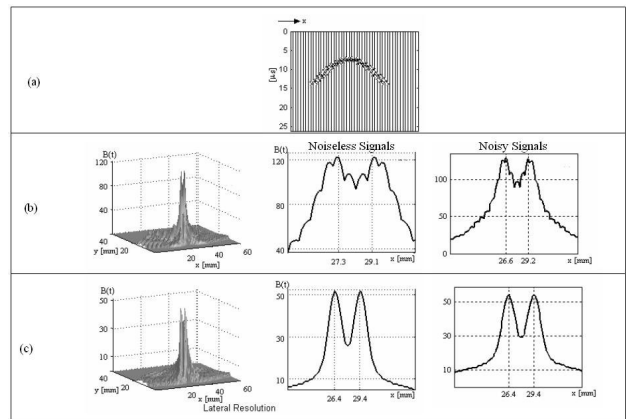


FIGURE 12. Two target lateral resolution for $r_p = 1.5\lambda$: a) simulated signals, b) classical beamformer output and c) envelope beamformer results.

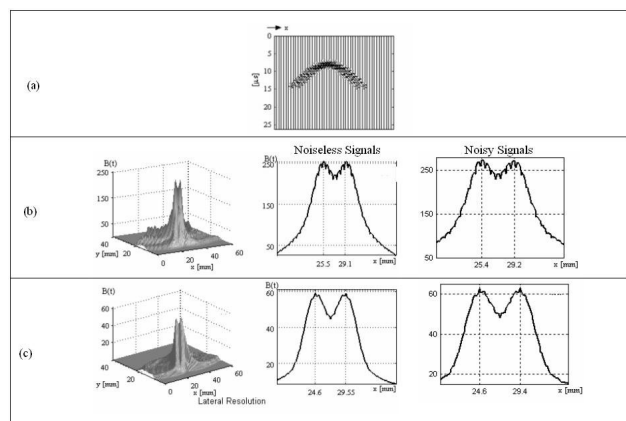


FIGURE 13. Two target lateral resolution for $r_p = 3\lambda$: a) simulated signals, b) classical beamformer output, and c) envelope beamformer results.

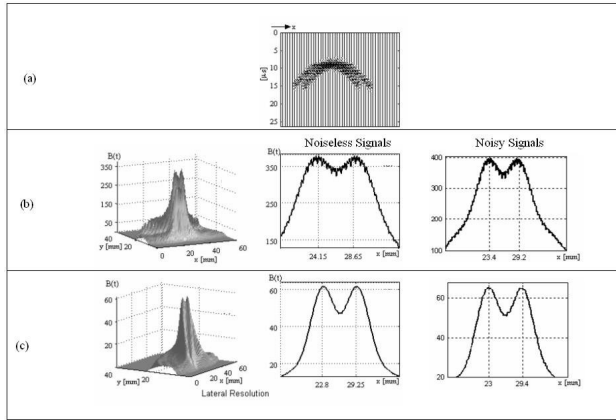


FIGURE 14. Two target lateral resolution for $r_p = 5\lambda$: a) simulated signals, b) classical beamformer output, and c) envelope beamformer results.

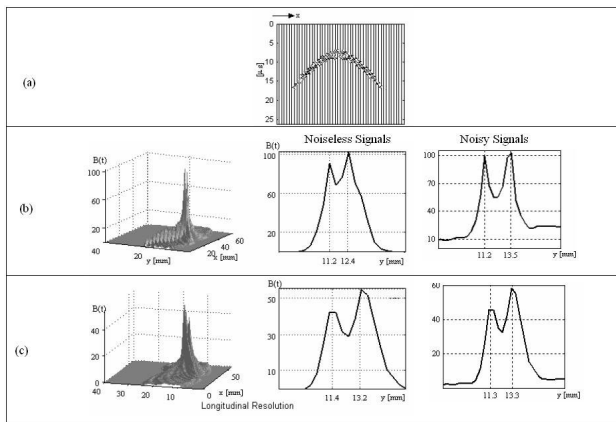


FIGURE 15. Two target longitudinal resolution for $r_p = 1.5\lambda$: a) simulated signals, b) classical beamformer output, and c) envelope beamformer results.

Figure 12 shows the lateral resolution when the pulse length is 1.5λ . The 3D meshes are the image produced by the beamformers, and the lateral resolution plots represent the profile along the x -axis of the maximal amplitude. In the plots, two peaks are well formed, almost of same amplitude, however the lateral resolution, while given by the classical algorithm is not as well-defined as the one produced by the present approach. The error in the T_2 position increases when the envelope beamformer is used to detect two targets. Once T_1 and T_2 target positions have been calculated, the lateral resolution is computed. From Table IV, can be seen that the calculated lateral resolution is smaller than the theoretical one, and the minimum distance between two targets is at least the double as the expected value. The lateral resolution is given by the classical beamformer, therefore it is closer to the theoretical value. The same behavior is produced when the pulse length is 3λ and 5λ , as shown in Fig. 13 and Fig. 14, respectively.

Longitudinal resolutions have been computed doing the same process as the lateral resolution calculation. The profiles of maximal amplitude along the y -axis, for different

TABLE V. Two targets longitudinal resolutions: a) Theoretical values, b) Classical and c) Envelope beamformers.

$r_p/2$ [mm]	r_y [mm]			
	Noiseless Signals		Noisy Signals	
(a)	(b)	(c)	(b)	(c)
0.9	1.2	1.8	2.3	2.0
1.8	1.2	4.0	3.6	3.4
3.0	4.8	4.8	4.8	4.4

TABLE VI. Two targets angular resolutions: a) Theoretical, b) Classical and c) Envelope beamformers.

(a)	θ_r [°]			
	Noiseless Signals		Noisy Signals	
(b)	(c)	(b)	(c)	
5.1	9.6	11.3	10.4	11.3
10.2	14.2	22.1	16.8	22.1
16.7	14.8	23.5	18.9	25.2

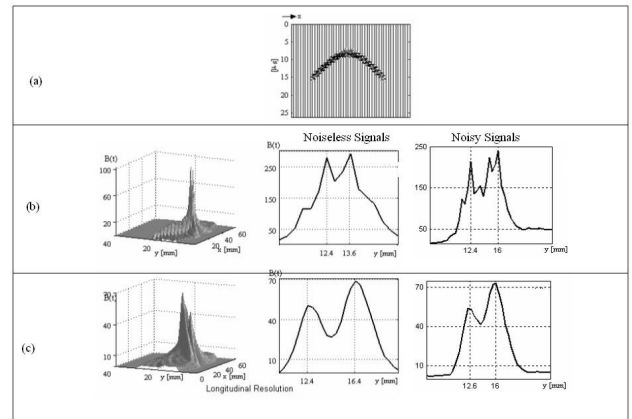


FIGURE 16. Two target longitudinal resolution for $r_p = 3\lambda$: a) simulated signals, b) classical beamformer output, and c) envelope beamformer results.

pulse lengths and noiseless/noisy signals, are plotted in Figs. 15, 16 and 17 and the resolution calculations are summarized in Table V.

The longitudinal resolution profiles produced by the classical technique are not smooth; in some cases (see Figs. 16 and 17) their number of peaks, of almost the same amplitude as the main lobe, also increase, their pulse length is larger and their signals are embedded in white noise. This behavior can lead to a wrong target location and way also provide false information about the number of targets in the scanned region. This is not the case when an envelope beamformer is used to locate targets. Table V shows the calculated and theoretical longitudinal resolutions. From this table, the distance between two targets is at least twice the theoretical minimum distance and much larger when the signals contain white noise.

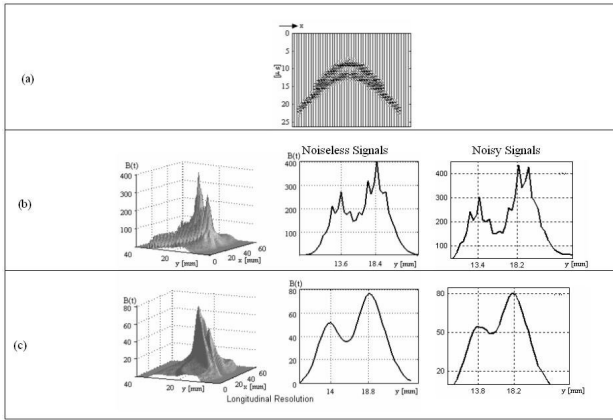


FIGURE 17. Two target longitudinal resolution for $r_p = 5\lambda$: a) simulated signals, b) classical beamformer output, and c) envelope beamformer results.

Once the range resolution has been computed and the targets positions calculated, the bearing resolution given by Eq. (11) can be determined as shown in Table VI. The minimum angle at the two targets can be located increasing as the pulse length increases, and also the classical beamformer bearing resolution is better than the time domain envelope algorithm, too. However, neither of them is within the theoretical bearing resolution.

5. Discussion and Conclusions

Classical and envelope beamformers for target locations are presented and their output results being compared.

The simulation is developed based on the time of flight information. Three pulse lengths and also the signals with additive white noise are considered. Classical and envelope beamformer algorithms are applied in each case, and the results have been presented for one and two targets.

The main advantage of envelope beamformer against classical algorithms is as follows:

The number of computational operations is reduced, since the summation in the present approach only considers the amplitude values at specific samples instead of first delaying the signals, and then summ them up with respect to the pulse length.

The single target detection and its location, for both algorithms applied to noiseless and noisy signals, are within the range resolution of the system. If the ultrasonic pulse length is larger, the error in a single target location does not change it, even within the range resolution of the system. However, the resulting images show some differences among the time-domain beamformers, such as:

- a) Spurious lobes amplitudes are present in the classical beamformer output, leading to false location and/or false number of detected in-homogeneities. If the pulse length increases, the lobes' amplitude increases too, and covers a larger region of the scanned space. If white noise is added to the received signals, then the

resulting images are drastically affected by the presence of sidelobes. So the resulting images of envelope beamforming algorithms show that the spurious lobes is harmless, and the region of maximal amplitude is around the target location.

- b) The profile shape of lateral resolution of both digital processes behave as a gaussian- window. Its maximum amplitude coincides with the target location, although the resulting profile when envelope beamforming is performed is narrower than the one produced by classical approach.

In order to find and compare the range and angular resolutions of the systems, for both algorithms, a second target has been positioned in the place of interest. The second target position is moved until the algorithms are able to detect it. The range and bearing resolutions defined as the minimum distance and the angle at which two targets can be detected by the systems are also computed. The calculated values are not within the expected values; they are at least two times the theoretical magnitudes, and the resulting images can be seen. The difference between classical and envelope beamformers outputs are:

- a) The minimum distance between the two targets is larger in the envelope beamformer approach. Therefore the angular resolution is smaller in the proposed approach.
- b) The spurious lobes, as in a single target case, are present in the beamformers outputs. These lobes are larger in the classical algorithm, producing false results, mainly when the pulse length is larger than 1.5λ .
- c) The lateral resolution profiles have a gaussian behavior, where the peaks, correspond to the targets. However the longitudinal resolution of the classical algorithm, when the pulse length is larger than 1.5λ , presents several sidelobes closer to the two mainlobes, producing false information about the number and position of the targets. This is not the case for the time-domain envelope beamformer, since its outputs produce two well-formed peaks, with no unwanted interference.

The main differences between the two algorithms are presented, so when a single target is in the region of interest, the error in the position measurement is within the expected values. However if a second target is added to the 2D space, neither of the algorithms' results is closer to the theoretical values. And the error increases for a large ultrasonic pulse length. In order to increase the range and bearing resolutions, a different envelope window must be chosen, such as a sharper envelope function. The pulse length must be shortened, too in order to find the optimum length.

Acknowledgments

The author would like to thank to Universidad Nacional Autónoma de México (PAPITT-IN105303) for its financial

grant, and to Mr. Francisco Javier Cárdenas Flores and Mr. Luis Alberto Aguilar Beltrán for their technical assistance.

-
1. D.W. Prine, *Proc Eng. Appl. Holog. SPIE* **287** (1972).
 2. P.D. Corl, G.S. Kino, C.S. Desilet, and P.M. Grant, *Acoust. Holog.* **8** (1980) 39.
 3. C.F. Scheuler, H. Lee, and G. Wade, *IEEE Trans. Sonics Ultrason.* **53** (1984) 195.
 4. L.J. Busse, H.D. Collins, and S.R. Doctor, "Review and discussion of the development of synthetic aperture focusing technique for ultrasonic testing (SAFT-UT)", Pacific Northwest Lab. Rep. NUREG/CR-3625, PNL-4957 (1984).
 5. Rastello T., Vray D., Chatillon J., *IEEE Trans. Image Proc.* **8** (1999) 1309.
 6. A.V. Osetrov, *Ultrasonics* **38** (2000) 739.
 7. M. Lang and H. Ermert, *Biomedizinische Technik Band* **42** (1997) 108.
 8. K.L. Gammelmark and J.A. Jensen, *Proc.* **4686** (2002) 25.
 9. S.I. Nikolov, J.A. Jensen, R. Dufait, and A. Schoisswohl, *Proc. IEEE Inter. Ultrason. Symp.* (2002) 1585.
 10. R.G. Pridham and R.A. Mucci, *J. Acoust. Soc. Am.* **63** (1978) 425.
 11. R.A. Mucci, *IEEE Trans. Acoust., Speech, Sig. Proc.* **32** (1984) 548.
 12. V.D. Van Veen, K.M. Buckley, *IEEE Trans. ASSP Magazine* (1988) 4.
 13. J.R. Williams, *J. of the Acoust. Soc. of Am.* **44** (1968) 1454.
 14. C.A. Balanis, *Antenna Theory: Analysis and Design*, (Harper Row Publishers, Inc., New York, 1982).
 15. W.S.H. Munro, *Ultrasonic Phased Arrays for use in Imaging and Automatic Vehicle Guidance*, (Ph. D. Thesis, Nottingham University, 1990).
 16. Y. Ozaki, H. Sumitani, T. Tomoda, and M. Tanaka, *IEEE Trans. Ultrason. Ferroelect. Freq. Contr.* **35** (1988) 828.
 17. D.H. Johnso and D.E. Dudgeon, *Array Signal Processing: Concepts and Techniques*, (Prentice Hall Inc., New Jersey, 1993).
 18. M. Born and E. Wolf, *Principles of Optics: Electromagnetic Theory of Propagation, Interference and Diffraction of Light*, (4th ed., Pergamon Press Ltd., London, 1970).
 19. P. Webb and C. Wykes, *IEEE Trans. Robotics and Autom.* **12** (1996) 138.
 20. L. Medina and C. Wykes, *Ultrasonics* **39** (2001) 19.
 21. E.G. Steward, *Fourier Transform: An Introduction*, (John Wiley & Sons, Inc., New York, 1983).
 22. R.A. Serway, *Physics for Scientists and Engineers: with Modern Physics*, (3th ed., Saunder College Publishing, Philadelphia, 1992).
 23. R.A. Gabel and R.A. Roberts, *Signals and Linear Systems*, (2nd ed. John Wiley and Sons, Inc., New York, 1980).
 24. B.P. Lathi, *Modern Digital and Analog Communication Systems*, (2nd ed., Holt, Rinehart and Winston, Inc., Philadelphia, 1989).
 25. A.B. Carlson, *Communication Systems: An Introduction to Signals and Noise in Electrical Communication*, (McGraw-Hill, Inc., New York, 1968).